Nuclear Instruments and Methods in Physics Research A 729 (2013) 77–84

Contents lists available at ScienceDirect

Nuclear Instruments and Methods in Physics Research A

journal homepage: www.elsevier.com/locate/nima

CALIFA Barrel prototype detector characterisation

B. Pietras [a,*], M. Gascón [a,f], H. Álvarez-Pol [a], M. Bendel [b], T. Bloch [d], E. Casarejos [g], D. Cortina-Gil [a], I. Durán [a], E. Fiori [e], R. Gernhäuser [b], D. González [a], T. Kröll [d], T. Le Bleis [b], N. Montes [a], E. Nácher [c], M. Robles [a], A. Perea [c], J.A. Vilán [g], M. Winkel [b]

[a] Universidade de Santiago de Compostela, E-15782, Spain
[b] Technische Universität München, 80333, Germany
[c] Instituto de Estructura de la Materia, CSIC, E-28006 Madrid, Spain
[d] Technische Universität Darmstadt, D-64289 Darmstadt, Germany
[e] Gesellschaft für Schwerionenforschung (GSI), D-64291 Darmstadt, Germany
[f] Lawrence Berkeley National Laboratory, 1 Cyclotron Rd. Berkeley, CA 94701, USA
[g] Universidade de Vigo, E-36310, Spain

ARTICLE INFO

Article history:
Received 4 April 2013
Received in revised form
3 June 2013
Accepted 17 June 2013
Available online 26 June 2013

Keywords:
Calorimetry
Scintillator materials
CALIFA
R^3B
Avalanche photodiodes
CsI(Tl)

ABSTRACT

Well established in the field of scintillator detection, Caesium Iodide remains at the forefront of scintillators for use in modern calorimeters. Recent developments in photosensor technology have lead to the production of Large Area Avalanche Photo Diodes (LAAPDs), a huge advancement on traditional photosensors in terms of high internal gain, dynamic range, magnetic field insensitivity, high quantum efficiency and fast recovery time. The R^3B physics programme has a number of requirements for its calorimeter, one of the most challenging being the dual functionality as both a calorimeter and a spectrometer. This involves the simultaneous detection of ~300 MeV protons and gamma rays ranging from 0.1 to 20 MeV. This scintillator – photosensor coupling provides an excellent solution in this capacity, in part due to the near perfect match of the LAAPD quantum efficiency peak to the light output wavelength of CsI(Tl). Modern detector development is guided by use of Monte Carlo simulations to predict detector performance, nonetheless it is essential to benchmark these simulations against real data taken with prototype detector arrays. Here follows an account of the performance of two such prototypes representing different polar regions of the Barrel section of the forthcoming CALIFA calorimeter. Measurements were taken for gamma–ray energies up to 15.1 MeV (Maier-Leibnitz Laboratory, Garching, Germany) and for direct irradiation with a 180 MeV proton beam (The Svedberg Laboratoriet, Uppsala, Sweden). Results are discussed in light of complementary GEANT4 simulations.

1. Introduction

A powerful technique which has revitalised nuclear physics exploration in recent years is use of inverse kinematics with relativistic, radioactive beams. The fleeting existence of such nuclei at the limits of stability necessitates transportation at the highest possible beam energies. Accordingly, the experimental setup for the Reactions with Relativistic Radioactive Beams, 'R^3B' physics programme must employ a calorimeter at the reaction target which accounts for the relativistic effects of Doppler broadening and shift inherent to a nominal beam energy of 700 A MeV.

This paper is motivated by the development of CALIFA [1], a scintillator based calorimeter to be housed at the future FAIR facility [2]. The calorimeter is divided into two sections, a 'Forward EndCap' covering polar angles between 7° and 43.2° and a cylindrical 'Barrel' section that ensures angular coverage up to 140.3°. The prototypes reported here correspond to different polar regions of the Barrel section.

The ambitious physics programme proposed for the R^3B facility dictates a set of requirements for the intended calorimeter as diverse as they are demanding [3]. This has motivated an extensive research and design campaign to optimise performance in every aspect of the calorimeter, reflected in the design choices taken for the prototypes characterised in this paper. A dedicated simulation campaign undertaken using the R3BRoot analysis framework [4], incorporating GEANT4 [5], has served as an indispensable guide to the development process.

The two prototypes here reported upon, denoted 'Section A' and 'Section B', are of respective geometries relating to different sections of the CALIFA Barrel. The polar region in the calorimeter to which each prototype corresponds is illustrated in Fig. 1.

At the heart of any successful calorimeter are two simple components; the scintillator and the photosensor. Regarding first

* Corresponding author. Tel.: +34 651189142.
E-mail address: benjamin.pietras@usc.es (B. Pietras).

0168-9002/$ - see front matter © 2013 Elsevier B.V. All rights reserved.
http://dx.doi.org/10.1016/j.nima.2013.06.063

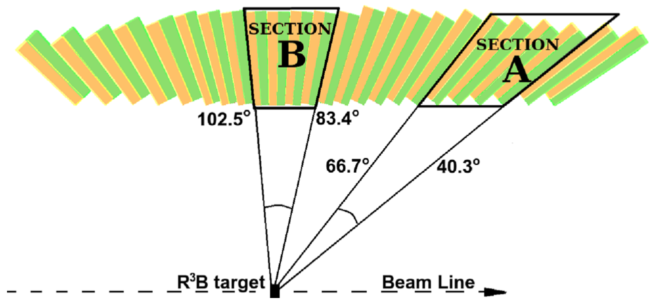

Fig. 1. A visualisation of the Barrel section of the forthcoming CALIFA calorimeter. Different colours denote the crystal type in the chiral pair (two pairs tessellate to fit four crystals to each alveoli). Note the variation of crystal opening angle and length as a function of polar angle. The prototypes correspond to each section as indicated. (For interpretation of the references to colour in this figure caption, the reader is referred to the web version of this article.)

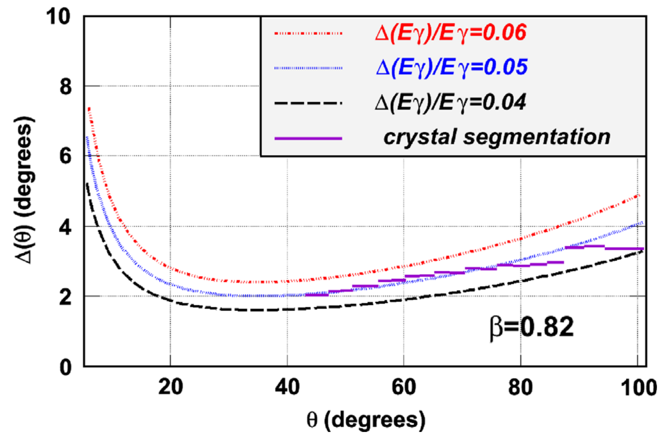

Fig. 2. The geometrical limitation on energy resolution for the R^3B physics programme nominal value of $\beta=0.82$. CALIFA segmentation is dictated by a 5% minimum, as can be seen by the crystal opening angles overlaid.

the scintillator, for the CALIFA Barrel section CsI(Tl) has been selected. As a scintillation material it offers a number of advantageous properties suited to our purpose: low hygroscopy, high stopping power, high light output in the green-yellow region of the spectrum and good energy resolution [6–8]. However, these positive attributes can be capitalised upon by coupling this established material to recently developed large area avalanche photodiodes, 'LAAPDs'.

Good energy resolution is integral to the performance of a calorimeter and even more crucial for a spectrometer. This combination of scintillator and photosensor is well suited to support such cases as the LAAPD quantum efficiency is not only exceptionally high, but also a near-perfect match to the light output wavelength of CsI(Tl). The combination of these properties is reflected in the good energy resolution measurement of 4.42% at 662 keV achieved via the coupling of a 1 cm^3 CsI(Tl) with a Hamamatsu S12102 LAAPD [9].

A further consideration is the close proximity of the final calorimeter to the forthcoming 4.8 Tm GLAD magnet, the fringe fields of which could distort photosensor operation, PMTs for example requiring shielding. LAAPDs are suitable for use in this environment as they are impervious to magnetic field effects.

One of the most challenging requirements of the R^3B physics programme is the simultaneous measurement of 0.1 MeV gamma rays and proton energies in excess of 300 MeV. Once more the CsI (Tl) – LAAPD combination is outstanding; where most traditional photosensors would struggle with the high photon flux, this combination finds no issues with saturation, enabling detection over a huge dynamic range whilst retaining good energy resolution.

Absorption of high energy protons and gamma-rays requires a greater length of scintillator material. At the R^3B nominal beam energy of 700 A MeV, such emissions observed in the laboratory frame will be increasingly Lorentz boosted in energy with the reduction of the polar angle of emission (θ). Therefore, in the conversion from the laboratory frame to the particle rest frame any uncertainty in θ imposes a geometrical limitation on the energy resolution. This Doppler broadening is in turn dependent on the polar angle itself. These requirements dictate the detector segmentation and length across the polar range of the calorimeter. The angular dependence is illustrated for different energy resolution values in Fig. 2, further details of which can be found in Ref. [10]. Here θ refers to the polar angle from the beam line at the R^3B target, while $\Delta(\theta)$ represents the angular uncertainty on the polar angle. The crystal segmentation is shown also, corresponding to the 5% at 1 MeV energy resolution requirement of the R^3B physics programme [3].

As seen in Fig. 2 the geometrical limitation on energy resolution can be improved by increasing detector segmentation. However, the inclusion of further passive material decreases calorimeter efficiency and promotes the fraction of protons traversing between scintillator elements. In any case, the intrinsic energy resolution of CsI(Tl) limits the improvement from further segmentation to much below 5% at 1 MeV. Other scintillators are available with superior intrinsic energy resolution, though these tend to be highly hygroscopic – the additional encapsulation required degrading the summed energy signal for inter-crystal scattered protons. The CsI(Tl) granularity has been optimised in such a manner as to ensure that the final resolution is not dominated by Doppler broadening, but close to the intrinsic resolution of the scintillation material, within the R^3B energy resolution requirements.

The two experiments here addressed regard the detection of high energy gamma rays at the Maier-Leibnitz Laboratory, Garching, Germany (MLL), and the measurement of high energy protons at The Svedberg Laboratoriet, Uppsala, Sweden (TSL), respectively. Each set of experimental data serves both as a validation of the GEANT4 simulations and an investigation into the response of different calorimetric sections under realistic experimental conditions.

2. High energy gamma rays, MLL

2.1. Experimental overview

Under investigation at the Maier-Leibnitz Laboratory, Garching, was a prototype detector which corresponded to the forward orientated 'Section A' of the CALIFA Barrel [1]. The MLL tandem accelerator was used to impinge 24 MeV protons onto a 12 mm carbon target. The resulting target excitation includes a significant population of the 2_1^+ and 1_2^+ excited states, which decay via the emission of gamma rays of 4.4 and 15.1 MeV, respectively. The detector was positioned at a polar angle of 37° from the beam, at a distance of 290 mm from the target. Aluminium shielding of a 4 mm thickness was employed to remove the elastic and inelastic scattered protons incident on the detector, as seen in Fig. 3.

2.2. Section A prototype

The Section A prototype consists of 16 CsI(Tl) truncated pyramidal crystals[1] in a 4×4 array, each crystal with an opening face of 12.2×23.2 mm, tapered to an exit face of 17×32 mm along a length of 180 mm. The exit face dimensions are well matched to the Hamamatsu S12102 'double' LAAPDs employed, which consist of

[1] Supplied by Amcrys Ltd.

two 10×10 mm LAAPDs paired with regards to similar optimum bias voltage and mounted in a common frame with a common voltage and readout. The LAAPDs were coupled to the crystals using Scionix RTV 861 optical cement [11]. Each crystal was wrapped with a single layer of a 65 μm thick ESR 'Enhanced Specular Reflector' optical wrapping [12] tailored to fit the crystal faces; this wrapping was found to yield superior energy resolution following the investigation of several candidates [13]. A photograph of four crystals wrapped in ESR and coupled to double LAAPDs is shown in Fig. 4.

Coupling a double LAAPD to each crystal was found to hold a number of advantages over the use of a single LAAPD unit. First, doubling the photosensor area significantly increases the fraction of collected light, yielding an increase of signal amplitude. This enables a substantial reduction of trigger thresholds, especially with regards to external noise sources which is of particular importance in larger systems. This allows to extend accurate measurement to a lower energy range and is also beneficial for calorimetric properties where an add-back procedure is employed. An add-back procedure is used to recover the energy of events with interactions distributed across several detectors, typically via the summing of detector energies within a selected region, providing each energy detected is above a threshold set to avoid the inclusion of low-level noise. Ergo, this threshold reduction enables an important improvement in the energy recovered.

A further factor is the single crystal energy resolution: on average an improvement of 10% in comparison to the single APD. A larger readout area is also expected to reduce the effect of non-linearity in the crystal as fewer reflections occur on average for the light collection. Finally the use of double LAAPDs holds the advantage that in the case that one of the LAAPD pair should fail mid-experiment, the energy deposited in that crystal can still be recovered.

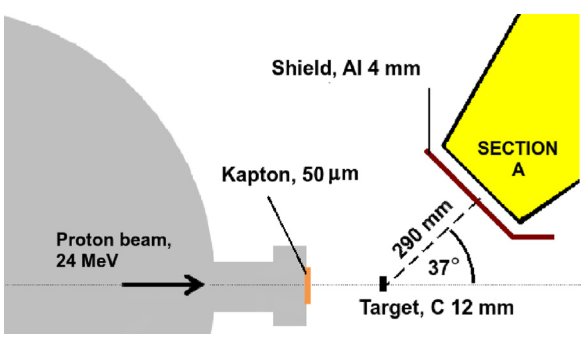

Fig. 3. Schematic of the setup at MLL, irradiation of the ^{12}C target with 24 MeV protons used to produce gamma ray emissions up to 15.1 MeV.

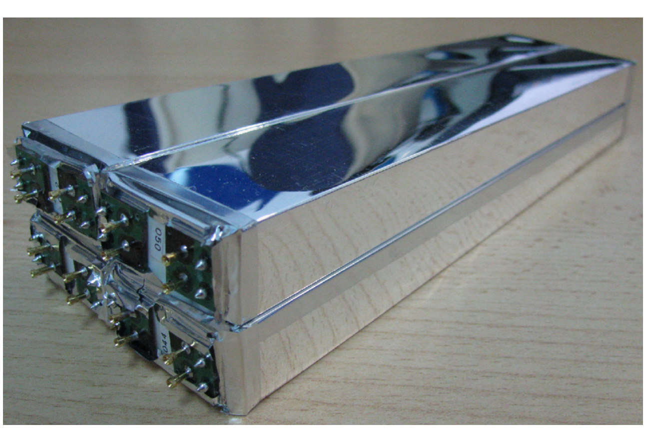

Fig. 4. A photograph of four CsI(Tl) crystals, wrapped in a single layer of ESR [12] and coupled to double LAAPDs. Each set of four consists of two chiral pairs, which tessellate to fit as fours into the alveoli honeycomb support structure (not shown).

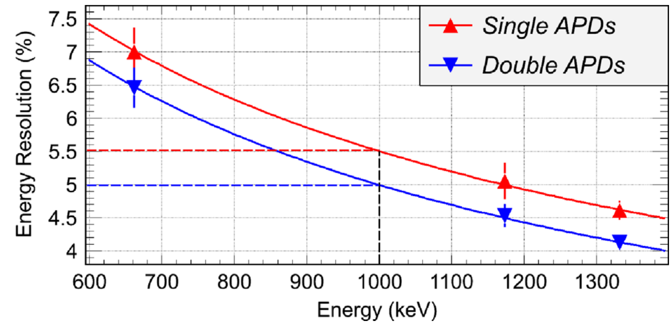

Fig. 5. Energy resolution values taken for standard calibration sources using 180 mm CsI(Tl) coupled to both 10×10 mm single and 10x20 mm double LAAPDs. Values taken from repeat measurements at our laboratory over a set of eight crystals for each case.

Shown in Fig. 5 are energy resolution measurements taken at our laboratory using CsI(Tl) crystals of a 12.2×23.2 mm entrance face, tapering over a 180 mm length to a 16.91×32.16 mm exit face; coupled respectively to 'single' (10×10 mm) and 'double' (10×20 mm) Hamamatsu LAAPDs. As can be seen, the double LAAPDs provide a consistently better energy resolution over the range measured, with the single LAAPD option slightly exceeding the R^{3}B physics programme energy resolution requirement of 5% at 1 MeV.

To hold these crystals within the calorimeter there are two major considerations: rigidity and minimisation of dead material. These are achieved via the use of a honeycomb of carbon fibre alveoli, minimizing dead material to optimize detector efficiency, as well as reducing energy loss for inter-crystal proton events. Each crystal was held as a set of four within a 500 μm thick carbon fibre alveoli, each set comprised of two chiral pairs. Recent advancements post-prototype have enabled a further reduction of carbon fibre thickness to 250 μm, pushing the limits of necessary structural strength.

At the MLL the setup employed a specially developed charge-sensitive preamplifier, the Mesytec MPRB-16, adapted to the high capacities of LAAPDs and contributing a relatively small amount of electronic noise. The MPRB-16 modules also featured a real-time temperature dependent gain adjustment, which may be set independently or as a common value for each channel. This temperature stabilisation is realised in an analogue way to a very high precision, below 0.1 °C. In comparison, the slow-control temperature measurement can only be precise to 0.2 °C in the best case [1]. For signal amplification the setup employed Mesytec MSCF-16 modules with a 4 μs time constant relating to the CsI(Tl) response, supported by a 32-channel VME multi-event peak sensing ADC (CAEN V785) with a 12-bit resolution and fast conversion time.

2.3. Experimental results

In consideration of the aforementioned relativistic effects in the R^{3}B setup, recovery of high energy gamma events is of particular importance. To investigate this capability, an external carbon target, 12 mm thick, was irradiated with a 24 MeV proton beam. These reactions induce significant population of the 2_1^+ and 1_2^+ ^{12}C excited states that prompts dominant gamma-ray decays at 4.4 and 15.1 MeV, respectively. The resultant gamma spectra, following calibration and an add-back procedure, can be seen in Fig. 6.

As evident in Fig. 6, gamma rays such as the lower intensity 8.3, 9.6 and 15.1 MeV decays, do not exhibit a clear photopeak as for the 4.4 MeV decay. This can be attributed to these higher energy decays requiring a greater volume of active material for full absorption: a phenomenon which will be explored at greater depth in the following simulations section.

Calibration at higher energy must be extrapolated from the fitting of a lower energy range as the range of standard gamma source energies only extends to a few MeV. Therefore linearity is a quality most desirable for this scintillator–photosensor combination. Good linearity can be seen for a sample of crystals in Fig. 7, where the $^{12}C\ 2_1^+$ decay 4.4 MeV full-energy peak and corresponding single and double escape peaks were used in addition to standard gamma-ray sources to perform the calibration. Linearity at much higher energies will be reported in the high energy proton section.

Such a high energy gamma ray as the 15.1 MeV photon provokes a prolific number of interactions within the detector material. Energy resolution at such high energies is degraded by bremsstrahlung emitted by the $e^{-/+}$ pair, generated mainly in the first interaction [14]. Despite the high stopping power of CsI, at this energy scattering across a large volume of scintillator material is inevitable. Recovery of the initial photon energy therefore necessitates summing the scattered energy across the prototype taking each crystal energy over a threshold of 50 keV. At this range of energy however, gamma events largely escape total absorption within the 4×4 active crystal array.

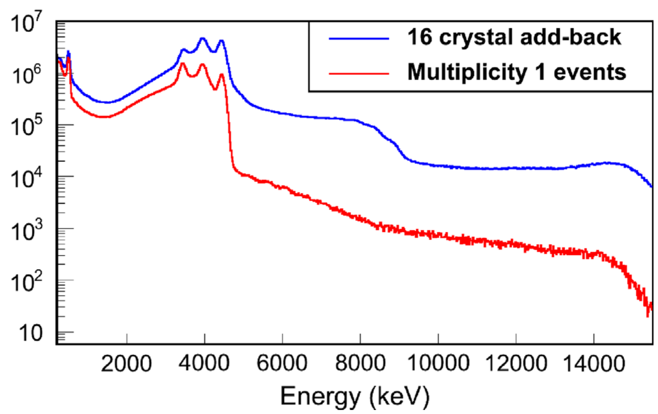

Fig. 6. Gamma spectrum following the de-excitation of ^{12}C. Shown are spectra following add-back and for the case where only a single crystal was struck (energy threshold set at 50 keV).

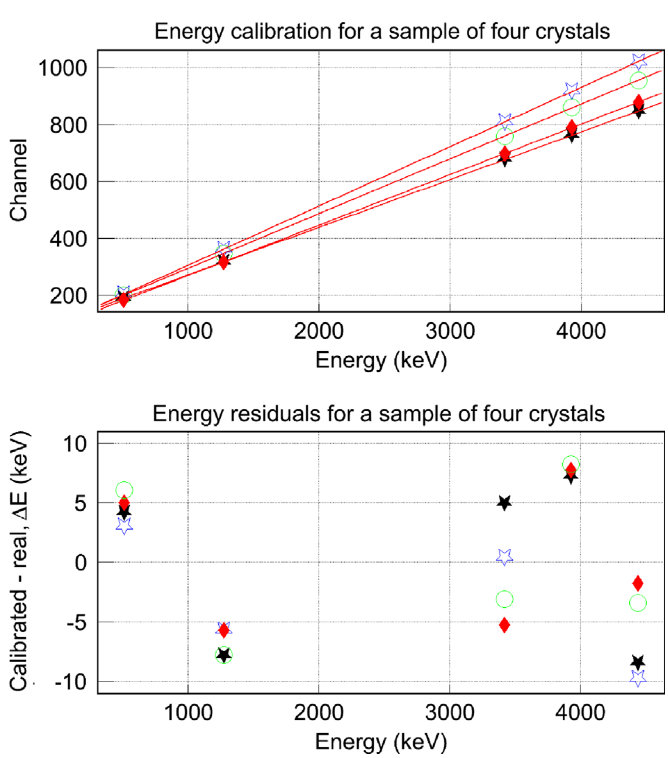

Fig. 7. Upper: a sample of four CsI(Tl) + LAAPD detectors with ^{22}Na and the 4.44 MeV full energy, escape and double-escape peaks from the proton irradiated ^{12}C, demonstrating good linearity up to 4.4 MeV. Lower: the residuals following this calibration, each symbol referencing a single crystal.

2.4. MLL Section A prototype simulations

De-excitation of ^{12}C produces prominent gamma rays at 4.4 and 15.1 MeV. The 4.4 MeV emission is useful to determine detector response in terms of energy resolution, realistic background and the crystal multiplicity dependence on energy, while the 15.1 MeV gamma highlights the challenges present in the recovery of such a high energy event.

Shown in Fig. 8 (upper) is a comparison of the experimental data 4.4 MeV peak with R3BRoot simulations. Two different energy resolution settings were simulated and displayed with the data. A realistic linear background from higher energy events was included in the simulations.

Table 1 is a comparison of both experimental and simulated results. A value of 8%, relating to the resolution at 1 MeV scaled with $\sqrt{E}$, was found to best match the experimental data in terms of energy resolution, following respective background fitting and subtraction.

Although an energy resolution of 8% at 1 MeV was found for the MLL data it should be noted that the same crystal geometry and LAAPD combination as the Section A prototype was found to have an energy resolution of 5% at 1 MeV, as seen previously in Fig. 5. This discrepancy could be explained by electrical cross-talk, insufficient grounding or use of non-optimum preamplifier settings: further investigation is required.

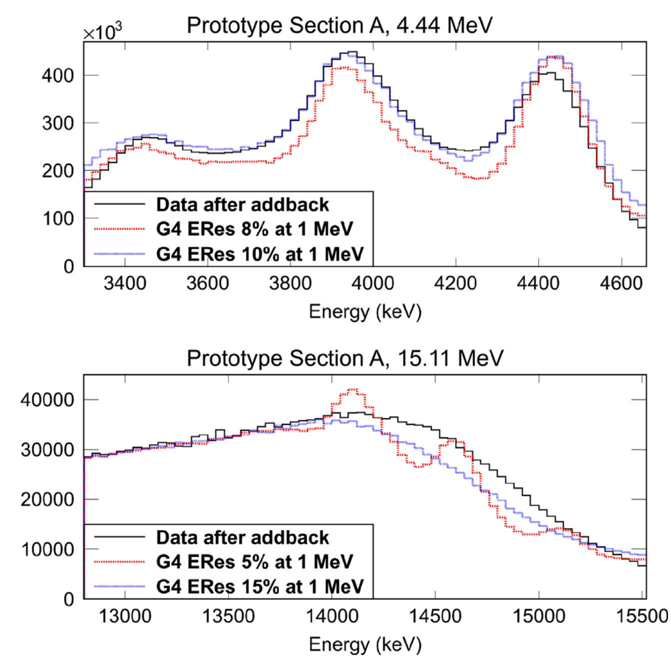

Fig. 8. Upper: a comparison of the experimental data 4.44 MeV gamma (solid line) with simulations of two energy resolution settings scaled with $\sqrt{E}$ from 1 MeV of 8% (red, dotted line) and 10% (blue, dashed line). Lower: a comparison of the experimental data 15.11 MeV gamma (solid line) with simulations with two energy resolution settings scaled with $\sqrt{E}$ from 1 MeV of 5% (red, dotted line) and 15% (blue, dashed line). The full-energy and escape peaks are apparent only for the 5% case.

Table 1
Energy resolution of the 4.44 MeV full energy peak, both for experimental data and R3BRoot simulations over a range of energy resolution settings.

Source	E_{res}(%) at 1 MeV	E_{res}(%) at 4.44 MeV
Data	–	3.50
Sim	7	3.17
Sim	8	3.62
Sim	9	3.97
Sim	10	4.68

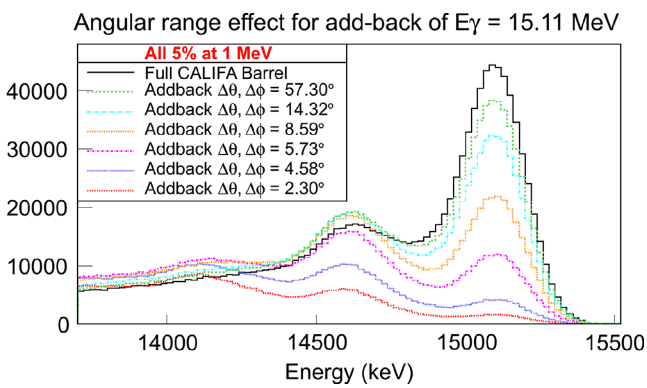

Fig. 9. Simulations of the CALIFA Barrel calorimeter for isotropic 15.11 MeV gamma emission with clustering taken for a selection of different angular windows. The volume dependence is evident; the number of crystals included in the clustering window greatly affects the photopeak recovery at such a high energy. The Section A prototype can be approximated to a clustering window of 4.58°. The resolution was set to 5% at 1 MeV in each case.

Performance in recovering high energy gamma rays is also crucial with regards to the spectroscopic requirement of CALIFA. In Fig. 8 (lower) is shown a comparison of simulations with different energy resolution settings overlaid upon experimental data. Only for the simulated energy resolution setting of 5% at 1 MeV can signs of the 15.11 MeV photopeak and escape peaks be observed with this limited set of 16 crystals. Reconstruction of the incident photon energy involved an initial determination of the crystal with the highest energy for that event. This is taken as the first point of interaction and set as the central point of an angular square window ($\Delta\theta$ and $\Delta\phi$) bordering a 'cluster' of crystals, within which any crystal energy over a 50 keV threshold is summed. The effect on photopeak recovery using an increasing number of scintillation crystals can be tested via simulations. The entire CALIFA Barrel was simulated for multiplicity one 15.11 MeV photons emitted isotropically. Add-back was performed over different angular clustering windows, the results displayed in Fig. 9.

The solid angle of the Section A prototype can be approximated to the clustering window of 4.58°, confirming that a volume of active scintillator material greater than that of the Section A prototype is necessary for high efficiency recovery of such high energy photon events. Analogous to Fig. 9, the results of multiplicity one, $\beta = 0$, simulations are shown for several gamma energies (0.1, 0.5, 1, 2, 5, 10 MeV) in Fig. 10, where the obtained photopeak efficiency is presented as a function of the angular clustering window.

Dominating interaction processes for high energy photons are pair production and Compton scattering, requiring a high volume of active material for complete photon absorption, corresponding to a large angular clustering window. Conversely, it is important to keep this clustering window as narrow as possible, as nuclear reactions frequently give rise to a gamma multiplicity higher than one, necessitating the use of separate clustering windows for each photon.

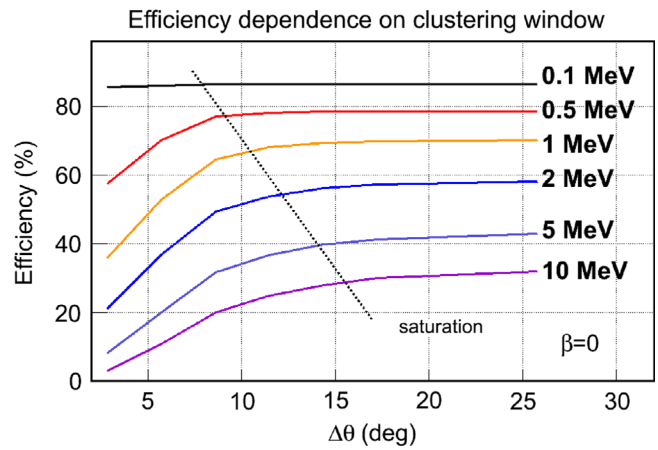

Fig. 10. CALIFA Barrel efficiency dependence of the clustering algorithm on the solid angle for add-back of various simulated energies (from top to bottom: 0.1, 0.5, 1, 2, 5, 10 MeV) [1]. Gamma events were emitted isotropically and with multiplicity one. A dotted line indicating saturation is included as a visual aid.

A simulation set was also performed using the R^{3}B nominal value of $\beta = 0.82$. It was observed that independent of the velocity of the source emitting the γ rays, there is a certain angular window for which the add-back algorithm saturates. This saturation shows a clear dependence on the energy of the photons, implying that the selection of a fixed angular parameter, not taking into account the energy detected in the crystal, might not be the most efficient way of reconstructing the energy of the events. One promising option for photon recovery is the use of an artificial neural network (ANN) [15]. For each event the ANN takes a number of parameters to best select the method for event reconstruction. Such parameters could include the crystal multiplicity, the maximum energy recorded by a single crystal, the total energy, the angle of the γ rays and the probability of interaction type within the crystal. The refinement of this method is reliant upon the R3BRoot simulation framework, while rigorous experimental verification of ANN methods will be possible with the aforementioned CALIFA Demonstrator. Development is ongoing and should provide a highly flexible and sophisticated method for reconstruction [16].

3. High energy protons, TSL

3.1. Experimental overview

The prototype array tested at The Svedberg Laboratoriet, Uppsala, Sweden (TSL) corresponded to a different section of the forthcoming CALIFA calorimeter, denoted as 'Section B' in Fig. 1. The Section B prototype consisted of 15 CsI(Tl) crystals wrapped with ESR and standard Teflon tape. This section is located at a 90° polar angle in the CALIFA design, reflected in the crystal geometry. The crystals have an entrance face of 29×10.4 mm^2 with a readout area well matched to the 10×20 mm^2 APD active area.[2] Crystal samples[3] were optically polished on all surfaces, the four crystals set in a 2×2 array within an Aluminium box employed both to avoid external light contamination and to electrically isolate the setup. The Section B prototype corresponds to a region of the CALIFA barrel set at a polar angle around 90°, greater than that of the more forward focused Section A prototype. Due to the Lorentz boost, the Section B angular region will be subject to gamma rays of a comparatively lower energy, which require a lower scintillator volume for full absorption. Reaction kinematics

[2] The Hamamatsu 68171 model, composed of two channels of S8664-1010.
[3] Provided both from Amcrys Ltd. and IMP Lanzhou.

dictate that protons emitted at this angle tend towards lower energies also. This is reflected in the Section B crystal length of 130 mm, compared to the Section A prototype crystal length of 180 mm.

The TSL accelerator was used to irradiate the Section B prototype directly with a 180.0 MeV proton beam, corresponding to what might be expected for that angular region of the forthcoming calorimeter under R^3B experimental conditions. Degraders were used to select further energy values of 120 and 92.7 MeV. After accounting for energy loss in layers of incident material, the beam energies of 92.7, 120 and 180 MeV correspond to proton energies of 84, 117 and 173 MeV reaching the active volume of the detector.

3.2. Experimental results

An example of the response of a single crystal for 173 MeV protons can been seen in Fig. 11.

The two prototypes share several common features, one notable exception being the use of Cremat CR-110 preamplifiers for the Section B prototype, with four mounted on a common card. The high proton energies supplied by the TSL accelerator would saturate these preamplifiers, necessitating the reduction of bias voltage on the LAAPDs to half the optimum value; thus degrading the energy resolution of the system. This was not an issue with the later MPRB-16 preamplifiers employed for the Section A prototype.

As previously noted, linearity of the detectors is highly important. Shown in Fig. 12 is the energy calibration for four crystals, demonstrating a good linearity over the measured range.

Despite technical difficulties limiting the active crystal cluster to a 2×2 crystal array, the inherent short-range scattering of protons ensured that a realistic performance measurement could be taken. The beam was defocused up to 40 mm in diameter so as to increase the impact area [17]. Double Sided Silicon Strip Detectors (DSSSDs), consisting of 32×32 perpendicular strips with a pitch of 1.86 mm and a thickness of 2 mm, were placed adjacent to the prototype to determine the position and dimensions of the incoming beam. An Aluminium box was used to electrically isolate the setup and to avoid any external light contamination.

Incident beam tracking with the DSSSDs opened an interesting feature to investigation: how did the proximity of the incident proton to the wrapping border between crystals affect the detector response? Highlighted in Fig. 13 (upper) are two regions, A and B, tagged for their energy response.

Region A corresponds to proton events which fall incident to the boundary between two crystals, while region B covers the central region of a single crystal. The boundary effect can be quite keenly observed in Fig. 13 (lower), which shows the reconstructed

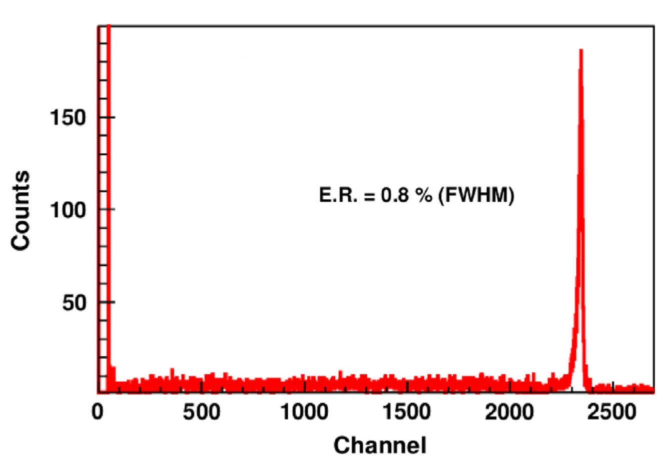

Fig. 11. Experimental data spectrum for a single crystal irradiated with 173 MeV protons.

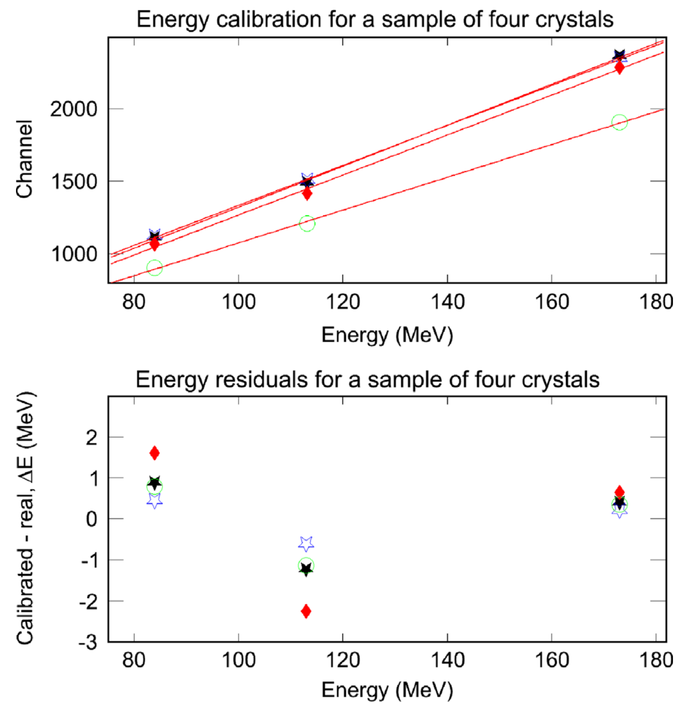

Fig. 12. Upper: calibration of proton energy for four crystals at energies of 84, 117 and 173 MeV. Lower: the residuals following this calibration, each symbol referencing a single crystal.

peaks for both indicated regions, along with the reconstructed peak using all events. Protons incident upon a border region between two crystals yield a peak with both a reduced mean energy and far inferior energy resolution than protons impinging on a central region of the crystal. These energy losses result from electrons generated in the proton path being stopped and absorbed in the wrapping material. The material traversed by the proton, X_t is dependent on the angle of entry via $X_t = X_n / \sin\,\theta$, characteristically small values of θ often leading to significantly greater values than the nominal material thickness, X_n. Whilst maintaining structural integrity, it is clear that the support structure and reflective wrapping of the crystals must be kept to an absolute minimum, dead material causing a reduction of detector efficiency and energy straggling for particles scattering between crystals.

Additional to the degraders, other layers of beam-incident material present introduced energy straggling to the proton measurement, worsening the energy resolution. To determine the energy resolution inherent to the detector crystals and support electronics alone, these contributions must be removed. This is easily accomplished by subtracting in quadrature the straggling effects, from a minor uncertainty of 0.06 MeV arising from the 100 μm stainless steel window to a significant 0.21 MeV from the DSSSDs. The uncertainty of ~0.34 MeV relating to the proton beam itself was also removed.

Despite the aforementioned minor degradation of energy resolution due to the use of sub-optimal APD bias voltages, following the subtraction we obtained $\sigma_{crystal+APD} = 0.35$ MeV, i.e. 0.47% FWHM for 173 MeV protons; well within the R^3B physics programme requirements [3].

3.3. TSL Section B prototype simulations

Since the commercial wrapping (ESR [12]) for the crystals had a thickness of 65 μm, dedicated simulations were run using values between 0 (vacuum) and four times 65 μm. Note that for a single layer of this material per crystal, the total thickness between two

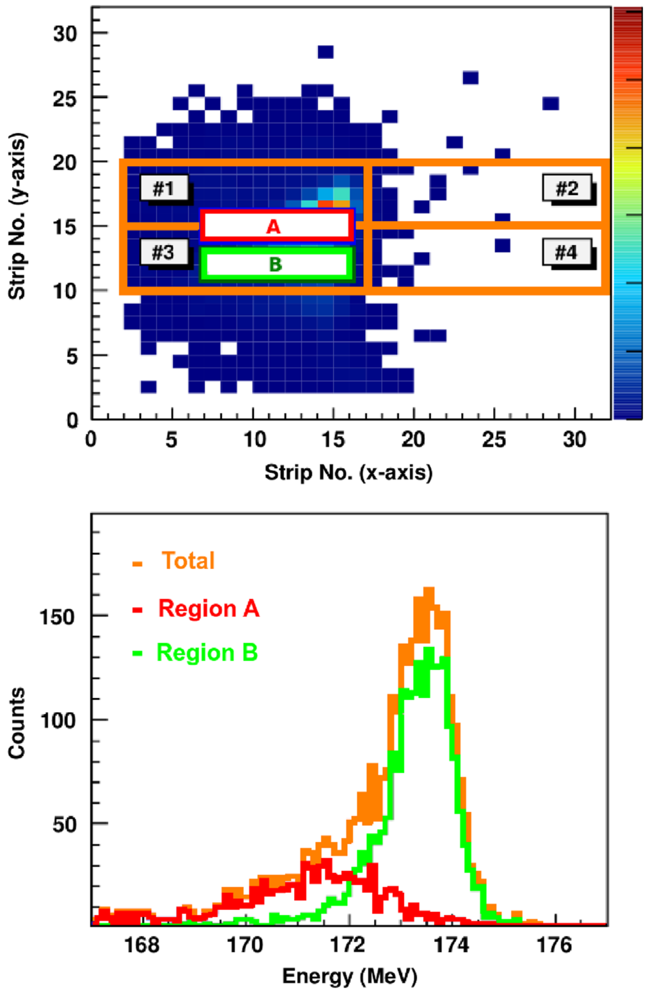

Fig. 13. Upper: the DSSSD, showing the 173 MeV proton beam profile incident on the Section B prototype. Lower: the resulting proton peaks from the DSSSD regions indicated, along with the reconstructed peak using all events. Protons striking the boundary region clearly yield a poorer energy measurement than those impinging central to the crystal.

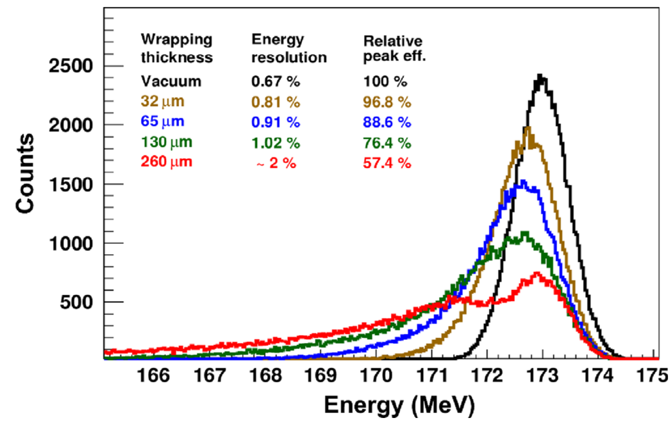

Fig. 14. Simulations of the energy peak observed for 173 MeV incident protons using different thicknesses of crystal wrapping. Shown is for crystal multiplicity 2 events.

crystals would be 130 μm. A double layer would increase this value to 260 μm. The simulations displayed in Fig. 14 indicates that the energy resolution was found to be around 1% FWHM for a wrapping thicknesses up to 130 μm, a value that fulfils the physics requirements for CALIFA.

In the case that the crystals are wrapped with a double layer, a secondary energy peak occurs, with a strong degradation of the energy resolution. The option to use a single layer of wrapping to separate two crystals was also investigated, however this is both difficult to seal correctly and vulnerable to direct light crosstalk from any defects or tears in the wrapping material. It should be noted that for the Section A prototype with a single layer of ESR wrapping used for each crystal the light crosstalk was measured at $0.24 \pm 0.07\%$. While ideally no crosstalk is desirable, in consideration of the detrimental effects of excess wrapping material, this level is quite acceptable.

4. Conclusions

The performance of two different prototypes representing sections of the CALIFA calorimeter have been investigated via the irradiation with medium-high energy protons (at TSL) and high energy gamma rays (at MLL). Various characteristics such as detector linearity and energy resolution have been quantified at these facilities, with accompanying measurements taken on-site at our laboratory with standard calibration sources.

Another area investigated was the effect of the wrapping and structural support matter on protons scattering between crystals. As predicted by simulation, this indeed significantly degrades the recovered full energy peak, confirming our approach to reduce the passive matter in the calorimeter design to an absolute minimum.

Of particular interest was the recovery of high energy gamma events, for which it has been confirmed via dedicated simulations that a greater volume detector than that of the existing prototypes is required. This will be recognised by the forthcoming CALIFA Demonstrator; a modular configuration of 8 petals, each comprised of 80 crystals. Covering a polar range of 32.5–65°, with 4 types of alveoli/crystals and 3 segments of 2 alveoli in the azimuthal direction and 10 alveoli in polar direction, the detector array will be 20% of the full Barrel into which it will be finally incorporated. With such a large volume of CsI(Tl) to recover the multiple scatters, the Demonstrator is expected to perform admirably in the recovery of very high energy gammas. Commissioning of the detector is planned for the first quarter of 2014.

The characterisation of these prototypes has served as a partial validation of the dedicated R3BRoot simulations, confirming the design's suitability to fulfil the R^3B physics requirements.

Acknowledgements

This work has been supported by FPA 2009, GANAS, ENSAR, HIC for FAIR, Mineco (FPA2009-14604-C02-01, FPA2009-07387), BMBF (06DA9040I, 05P12RDFN8, 06MT9156, 05P12WOFNF, 05P12WONUE), the Spanish Ministereo de Ciencia e Innovación (FP2005-00732) and the Xunta de Galicia (project number PGIDIT07PXIB206124PR).

References

[1] The CALIFA Collaboration, CALIFA Barrel Technical Design Report, 2012, approved Jan. 2013.
[2] The FAIR Collaboration, FAIR CDR – An International Accelerator Facility for Beams of Ions and Antiprotons, Conceptual Design Report., Technical Report, GSI, 2001.
[3] T. Aumann, B. Jonson, Technical Proposal for the Design, Construction, Commissioning and Operation of R3B, A Universal Setup for Kinematical Complete Measurements of Reactions with Relativistic Radioactive Beams, 2005.
[4] D. Bertini, Journal of Physics: Conference Series 331 (2011) 032036.
[5] S. Agostinelli, J. Allison, K. Amako, et al. Nuclear Instruments and Methods in Physics Research Section A 506 (2003) 250.

[6] P. Schotanus, R. Kamermans, IEEE Transactions on Nuclear Science NS-37 (1990) 177, http://dx.doi.org/10.1109/23.106614.
[7] M. Gascón, H. Álvarez-Pol, J. Benlliure, E. Casarejos, D. Cortina-Gil, I. Duran, IEEE Transactions on Nuclear Science NS-55 (2008) 1259.
[8] V.P. Semynozhenko, B.V. Grinyov, V.V. Nekrasov, Y.A. Borodenko, Nuclear Instruments and Methods in Physics Research Section A 537 (2005) 383, Proceedings of the 7th International Conference on Inorganic Scintillators and their Use in Scientific and Industrial Applications.
[9] M. Gascon, H. Álvarez-Pol, J. Benlliure, E. Casarejos, D. Cortina-Gil, I. Duran, IEEE Transactions on Nuclear Science NS-55 (2008) 1259–1262.
[10] H. Álvarez-Pol, J. Benlliure, E. Casarejos, D. Cortina, I. Durán, M. Gascón, Nuclear Instruments and Methods in Physics Research Section B 266 (2008) 4616.
[11] RTV 861, Scionix. Netherlands.
[12] ESR is a trademark of 3M, ⟨http://vikuiti.com⟩, 2003.
[13] M. Gascón, Prototype of a new calorimeter for the studies of nuclear reactions with relativistic radioactive beams, Ph.D. Thesis, Universidade de Santiago de Compostela, 2010.
[14] M. Bendel, R. Gernhäuser, R. Kürcken, T. Le Bleis, M. Winkel, Particle$-\gamma-$Separation with CALIFA, GSI Scientific Report, PHN-NUSTAR-NR-24, 2010.
[15] E. Yoshida, K. Shizuma, S. Endo, T. Oka, Nuclear Instruments and Methods in Physics Research Section A 484 (2002) 557.
[16] P. Teubig, Development of reconstruction algorithms for CALIFA, Ph.D. thesis, Universidade de Lisboa, 2012.
[17] D.D. DiJulio, V. Avdeichikov, J. Cederkall, P. Golubev, B. Jakobsson, H. Johansson, C. Tintori, Nuclear Instruments and Methods in Physics Research Section A 612 (2009) 127.